



Simulation study on light ions identification methods for carbon beams from 95 to 400 MeV/A

S. Samuel Salvador, M. Labalme, J.M. Fontbonne, J. Dudouet, J. Colin, D. Cussol

► To cite this version:

S. Samuel Salvador, M. Labalme, J.M. Fontbonne, J. Dudouet, J. Colin, et al.. Simulation study on light ions identification methods for carbon beams from 95 to 400 MeV/A. 2013. in2p3-00868025

HAL Id: in2p3-00868025

<https://hal.in2p3.fr/in2p3-00868025>

Preprint submitted on 1 Oct 2013

HAL is a multi-disciplinary open access archive for the deposit and dissemination of scientific research documents, whether they are published or not. The documents may come from teaching and research institutions in France or abroad, or from public or private research centers.

L'archive ouverte pluridisciplinaire **HAL**, est destinée au dépôt et à la diffusion de documents scientifiques de niveau recherche, publiés ou non, émanant des établissements d'enseignement et de recherche français ou étrangers, des laboratoires publics ou privés.

Simulation study on light ions identification methods for carbon beams from 95 to 400 MeV/A

S. Salvador*, M. Labalme, J.M. Fontbonne, J. Dudouet, J. Colin, D. Cussol

*Laboratoire de physique corpusculaire de Caen, ENSICAEN, 6 boulevard du Maréchal
Juin, 14050 Caen cedex, France*

Abstract

Monte Carlo simulations have been performed in order to evaluate the efficiencies of several light ions identification techniques. The detection system was composed with layers of scintillating material to measure either the deposited energy or the time-of-flight of ions produced by nuclear reactions between ^{12}C projectiles and a PMMA target. Well known techniques such as ΔE —Range, ΔE — E —ToF and ΔE — E are presented and their particle identification efficiencies are compared one to another regarding the generated charge and mass of the particle to be identified. The simulations allowed to change the beam energy matching the ones proposed in an hadron therapy facility, namely from 95 to 400 MeV/A.

Keywords: Hadron therapy, Particle Identification, Monte Carlo Simulations

*Corresponding author. Tel.: +33 2 31 45 25 54

Email address: salvador@lpccaen.in2p3.fr (S. Salvador)

1. Introduction

Particle identification is of major importance in multiple fundamental physics experiments and especially for nuclear reaction studies. Various methods can be used, mostly based on the Bethe-Bloch formula, to retrieve either the partial energy ΔE , lost in a thin detector, the total energy E in a thick one [1], the β parameter using the particle velocity based on time-of-flight (ToF) measurements [2], or the range [3–5] as well as the Bragg peak amplitude [6]. The associated detection system can be made of solid state detectors, such as germanium or silicon allowing very good estimation of the deposited energy and pulse shape discrimination [7, 8]; scintillating material, either organic or inorganic, for good timing resolution particularly in high energy physics [9]; or gaseous detectors as a low density stopping medium [10] for low kinetic energy ions. The detection system is then designed and optimized for the purpose of the technique used. It is thereby difficult to know *a-priori* the most efficient method for identification when designing a new experiment.

In this paper, we have performed simulation studies for particle identification in multi-fragmentation processes of carbon beams with targets at energies ranging from 95 to 400 MeV/A. We focused on three methods, based on ΔE —Range, ΔE — E —ToF and ΔE — E measurements done by scintillating detectors only. Solid state and gaseous detectors have been left aside due to their poor timing resolution (>1 ns) and too low density (~ 1 mg cm $^{-3}$), respectively. The detection system is the same for all measurements (save for the thickness of the thin stage) to be able to compare identification techniques and not the system performances.

26 The goal of this work is to investigate an efficient method able to dis-
27 criminate 1 atomic mass up to ^{12}C ions. The system will be used in double
28 differential cross-section measurement experiments for carbon therapy inter-
29 est, at the new Advanced Resource Center for HADron therapy in Europe
30 (ARCHADE) based in Caen.

31 2. Simulation materials and methods

32 The simulations were based on the GEANT4 Monte-Carlo toolkit [11].
33 The GEANT4 version used is the 9.5 with the physics list QMD (Quan-
34 tum Molecular Dynamics) for inelastic reactions associated with an FBU
35 (Fermi Break-Up) de-excitation process. This physics list has been chosen
36 instead of the current BIC (Binary Intra-nuclear Cascade) package due to its
37 cross-sections of fragments production closer to experiments, particularly for
38 energy distributions [12].

39 The simulations consisted on the interaction of 10^6 ^{12}C ions at normal
40 incidences with a spherical PMMA target of 5 mm in diameter performed
41 in ultra vacuum. For each event, the interactions of the primary particle or
42 secondaries with the detection system were recorded. For each ion, its Z and
43 mass value (A) are known and compared in the post processing analysis to the
44 measured one using different identification method, described in the following
45 sections. The system can detect events coming from the beam which have
46 not encountered any fragmentation processes in the target. These events are
47 the most likely ones. However, to avoid degradation of the results, data from
48 primary ions, i.e. encountering no inelastic processes in the target, were not
49 been used in the identification processes. This will be discussed separately

50 in the appropriate section.

51 Multiple simulations were done by changing the beam energy from 95 MeV/A
 52 (maximum energy provided by GANIL in Caen), to 200, 300 and 400 MeV/A,
 53 representing appropriate energies for carbon therapy purposes.

54

55 The simulated detection system was based on thallium doped cesium
 56 iodide scintillating crystals (CsI:Tl) with a density of 4.51 g cm⁻³, a decay
 57 time of 1 μ s and a light yield of ~ 55 ph keV⁻¹ [13]. This crystal has been
 58 chosen due to its known quenching factors, that allowed the conversion of the
 59 deposited energy into scintillation light for better accuracy. This conversion
 60 was made according to the formula given in [14]:

$$\begin{aligned}
 L = a_1 \Bigg\{ & E_0 \left[1 - a_2 \frac{AZ^2}{E_0} \ln \left(1 + \frac{E_0}{a_2 AZ^2} \right) \right] \\
 & + a_2 a_4 AZ^2 \ln \left(\frac{E_0 + a_2 AZ^2}{a_3 A + a_2 AZ^2} \right) \Bigg\}, \quad (1)
 \end{aligned}$$

61 where L is the scintillation light in equivalent number of photoelectrons,
 62 E_0 , the deposited energy in keV, a_1 , the conversion factor from energy to
 63 converted photoelectrons, $a_{\{2...4\}}$ are the quenching factors, A and Z , the mass
 64 and atomic number of the ion. Table 1 gives a summary of the quenching
 65 factors while a_1 represents in our case the light yield of the scintillator times
 66 the photon detection efficiency of the associated photodetectors. The photon
 67 detection efficiency is taken as the quantum efficiency ($\varepsilon_q = 0.25$) of the
 68 photodetector such as a photomultiplier tube, times the collection efficiency
 69 taken to be around 50%. In the following sections, energy will always be
 70 expressed as the measured output light, in terms of photoelectrons, even if

71 mentioned as energy.

Table 1: Values of the quenching factors used in the simulations [14].

| a_1 | a_2 | a_3 | a_4 |
|-------|-------|-------|-------|
| 6875 | 0.71 | 3.8 | 0.26 |

72 To introduce the detector energy resolution, each amount of converted
73 photoelectrons values were randomly extracted from a gaussian distribution
74 with L as mean value and sigma given by :

$$\sigma_L = \frac{L}{2.35} \times \left(\frac{1.021}{\sqrt{E_0}} + 0.019 \right). \quad (2)$$

75 The energy resolution parameters were derived from experimental energy
76 resolutions given by [15].

77 The detector was composed of scintillating layers of $120 \times 120 \text{ cm}^2$ and
78 increasing thicknesses. Each layer scaled with depth from 0.2 mm to 13 mm
79 thick by 0.2 mm steps to accurately sample the small ranges and to be able
80 to optimize the thickness of the ΔE stage. Using 65 layers, the total depth
81 of the detector is 42.9 cm allowing to entirely stop protons up to 480 MeV.
82 The thickness of the first stage is optimized by finding the minimum value
83 of number of layers which minimizes the identification errors. This basically
84 means that one need to maximize the deposited energy while minimizing the
85 number of inelastic interactions inside the corresponding material thickness.
86 Table 2 gives a summary of the optimized thicknesses (the sum of layers
87 thicknesses considered for the ΔE stage) used at the different energies for
88 the ΔE —ToF and ΔE — E methods.

89 The system was located at 2.4 m from the target offering a $\pm 13^\circ$ opening
90 angle and a good ToF measurement. Fig. 1 gives a schematic view of the
91 simulation set-up.

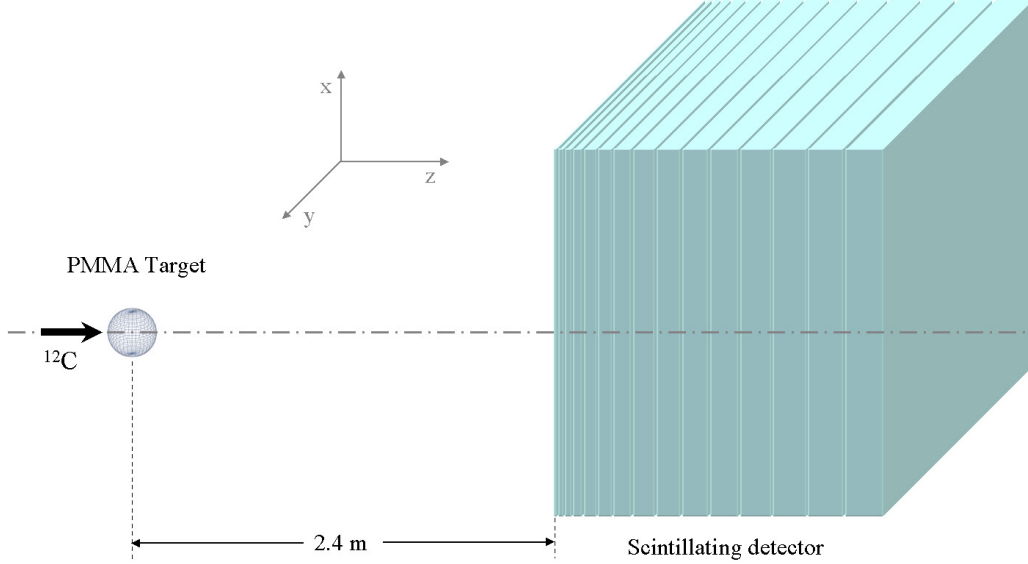


Figure 1: Schematic view of the detection system. Not at scale for clarity reasons.

Table 2: Thickness of the ΔE layer in mm at different beam energies.

| Beam energy (MeV/A) | Thickness (mm) | |
|------------------------|------------------------|-------------------------|
| | ΔE —ToF method | ΔE — E method |
| 95 | 0.2 | 0.6 |
| 200 | 0.6 | 1.2 |
| 300 | 0.6 | 2.0 |
| 400 | 2.0 | 2.0 |

92 Despite the fact that ions can easily be tracked in depth (in the z direc-

tion), tracking in the xy plane was not used except to distinguish the energy deposition by each individual ion. It is obvious that such a system is very unlikely to be built. First of all, the thicknesses of the layers, particularly at small ranges, should be increased to allow the fabrication process and the use of appropriate photodetectors. Then, each layer would be individually divided into small tills to have some tracking information in the xy plane. Some detection systems based on the same principle have already been tested for hadronic granular calorimetry dedicated to particle physics [16].

The following paragraphs will describe the techniques used for particle identification.

2.1. The E —Range method

The E —Range method is usually used for identification of particles with ranges measured in a gaseous detector within few tens of centimeters. Here, the method is presented to identify charged particles with much higher velocities detected in a dense material (density of 4.51 g cm^{-3}).

The relation between the energy and the range (eq. 3) has been derived from the Bethe-Bloch formula by Greiner [4] for β values under 0.7 which correspond approx. to 370 MeV/A.

$$E = a_1 A \left(\frac{b R Z^2}{A} \right)^c, \quad (3)$$

where a_1 is the conversion factor for energy to photoelectrons, b and c are fit parameters and R is the range.

By measuring simultaneously the total deposited energy and the range of an unknown ion, its charge and mass can be obtained.

115 *2.2. The ΔE — E —ToF method*

116 While the ΔE —Time-of-Flight method is used to measure the charge
 117 of ions, the Energy—ToF method can be used to obtain their mass. Using
 118 the Bethe-Bloch formula to obtain the charge dependence of the deposited
 119 energy in a Δx thin medium (eq. 4) and the relativistic equation of a particle
 120 total energy (eq. 5), one can adjust fit parameters to identify the ions in two
 121 different ΔE —ToF and E —ToF distributions.

$$\Delta E = a_1 \frac{Z^2}{\beta^2} \left[\ln \left(\frac{\beta^2 b_{mat}}{1 - \beta^2} \right) - \beta^2 \right] \Delta x, \quad (4)$$

122

$$E = a_1 b_{\{1...12\}} u A \left(\frac{1}{\sqrt{1 - \beta^2}} - 1 \right), \quad (5)$$

123 where b_{mat} is a fit parameter depending on the detector material, $\beta =$
 124 $\frac{d}{c \times ToF}$ with d , the distance to the detector, c , the speed of light, and u is the
 125 unified atomic mass of 931.494 MeV c^{-2} . This approximation stands due to
 126 the use of correction parameters $b_{\{1...12\}}$ obtained from the fit for each ion
 127 mass.

128 To introduce a measurement coincidence time resolution, ToF measure-
 129 ments are obtained from random values of a Gauss distribution where the full
 130 width at half maximum (FWHM) has been set to 300 ps. This value, even
 131 if not achievable using CsI:Tl crystals, can be measured with good timing
 132 detectors using fast scintillators and photomultiplier tubes [17].

133

134 One main disadvantage of these two techniques is that they relate in-
 135 dependently to the same particle due to the need of two different plots for

136 identification. This leads to some very unlikely isotopes identification coming
 137 from a mass value uncorrelated to a Z value. As a consequence, the given
 138 results only take into account isotopes supposed to be produced by the initial
 139 reaction between ^{12}C and nuclei in the target.

140 2.3. The ΔE — E method

141 The ΔE — E method is often used to identify charged particles even with
 142 energies up to few hundred MeV/A whether using gaseous, solid state or
 143 scintillating detectors for both measurements of ΔE or E . It relies on the
 144 detection of the energy deposited by particles in a thin detector as a function
 145 of the residual deposited energy in a sufficiently thick detector to stop the
 146 particle.

147 A usual functional of the relation between ΔE and the residual energy is
 148 given in [18] by:

$$\begin{aligned} \Delta E = & \left[(gE)^{1+\mu} + (\lambda Z^\alpha A^\beta)^{1+\mu} \right. \\ & \left. + \xi Z^2 A^\mu (gE) \right]^{\frac{1}{1+\mu}} - gE, \end{aligned} \quad (6)$$

149 with g , μ , λ , α , β and ξ are parameters obtained by fitting the distribu-
 150 tions for each couple (Z, A). The parameter λ includes the a_1 parameter as
 151 well as the thickness of the first stage, Δx .

152 2.4. Particle identification

153 Using the different analytical solutions given by the equations, identifica-
 154 tion of a particle was made for each method by a Newton-Raphson approach.
 155 In this case, the distance of an event to the curve was minimized in few steps,

156 making the event to be on the normal to the curve's tangent. An event was
 157 then attributed to a curve for the smallest event-to-curve distance when test-
 158 ing for all curves, relating the event to a particular Z and/or A value.

159 To compare the identification efficiency with the known ion charge and
 160 mass, distributions of the charge and the particle identification parameter
 161 (PID, taken as $0.8 \times Z + 0.1 \times A^1$) were built for both measured and real val-
 162 ues. The number of measured counts at a particular PID (N_{meas}) was then
 163 compared to the corresponding one in the generated distribution, N_{true} . The
 164 result was normalized by N_{true} to obtain the relative identification error (RIE,
 165 eq. 7). As a result, this method took into account all sources of identification
 166 errors but is also dependent on the isotope statistic.

$$RIE = \frac{|N_{meas} - N_{true}|}{N_{true}}. \quad (7)$$

167 2.5. Energy evaluation

168 For each method, the measured energy of a **well identified** particle
 169 ($PID_{meas} = PID_{true}$) is compared to the generated one. The energy can then
 170 be obtained either by the total deposited energy (or the sum of the par-
 171 tial and residual energy) or by time-of-flight measurements. Special care
 172 was taken when evaluating the energy by the ToF method. This one was
 173 obtained using a similar formula as eq. 5, except that the Z and A of the
 174 particles are known and that the proton and neutron masses as well as the
 175 binding energies can be used instead of the parameters $b_{1...12}$. The energy in
 176 MeV is then converted in photoelectrons using the parameter a_1 .

¹For instance, tritons have a PID equal to 1.1 and α particles have a PID = 2.0.

177 A plot is thereafter made summing all detected particles. The ratio of
 178 ions with a measured energy truncated due to losses after inelastic collisions,
 179 R_{trunc} , is extracted. First, the FWHM of the peak centered around 1 is
 180 evaluated. Assuming a gaussian distribution, a lower limit of -5σ (using
 181 $1\sigma = \text{FWHM}/2.35$) to the position of the peak is obtained. For each method
 182 and beam energy, the ratio is measured by summing the number of events up
 183 to the limit divided by the total amount of events in the distribution. This
 184 parameter evaluates then the effect of the method in the degradation of the
 185 ion energy even if this one has been well identified.

186 3. Results

187 3.1. Particle identification

188 Fig. 2 shows an example of the energy per nucleon distributions of the
 189 isotopes generated by the simulation and detected by the system for $E_{beam} =$
 190 400 MeV/A. At this energy, the distributions are well centered around the
 191 beam energy representing mostly fragments from the projectile, except for
 192 protons (PID = 0.9) and deuterons (PID = 1.0) which exhibit broader dis-
 193 tributions.

194 Figure 3 gives an example of the plots of the different identification meth-
 195 ods with their associated fitted curves at $E_{beam} = 400$ MeV/A. The color
 196 scales denote the number of events per bin and the energy is expressed as the
 197 number of collected photoelectrons. Dashed lines represent the curves used
 198 for identification.

199 Fig. 4 presents an example of the relative identification error for the three
 200 methods as the charge (Z) and the PID relative identification error. Values

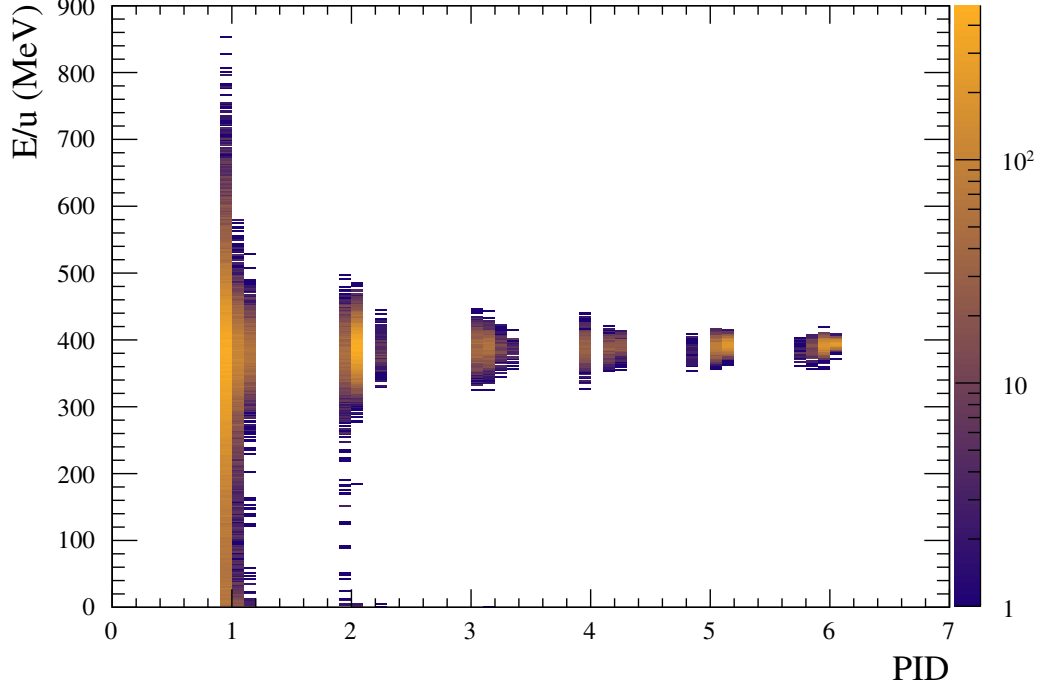


Figure 2: Energy distribution of the different detected isotopes for $E_{beam} = 400$ MeV/A.

201 higher than 100% refer to isotopes identified with a higher statistic compared
 202 to the generated one. This occurs when the pollution induced by heavier
 203 particles that have experienced an inelastic collision in the CsI layer is large
 204 compared to the statistic of the generated particles (see section 4 for details).

205 Table 3 summarizes the average relative identification errors for the meth-
 206 ods at the different beam energies and gives the highest value in the statis-
 207 tic. When identifying the charge of the ion, the ΔE —ToF is in average the
 208 most efficient method for any beam energy, with an efficiency above 95%
 209 ($RIE \leq 5\%$) for any charge. This is mainly due to the good timing resolution
 210 and the distance for the time-of-flight measurement while the other methods
 211 rely on the energy resolution of the system for this evaluation. When the

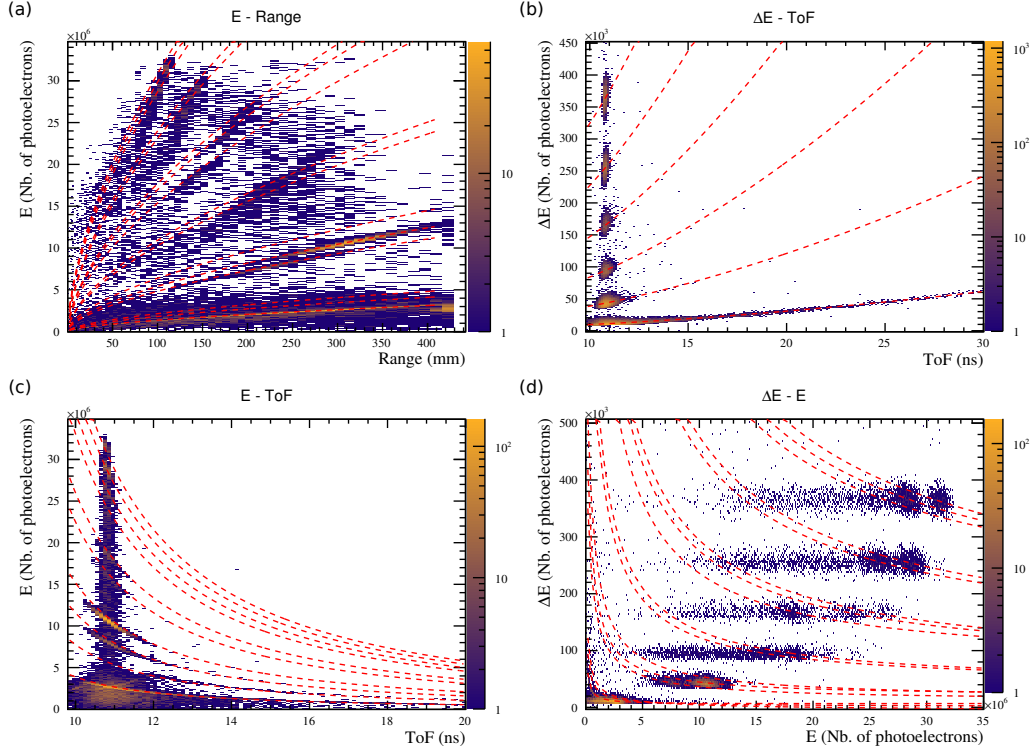


Figure 3: Distributions of (a) E versus range, (b) ΔE versus ToF, (c) E versus ToF and (d) ΔE versus the residual energy for a beam energy of 400 MeV/A. Red dashed lines represent the curves used for identification.

212 thickness of the ΔE stage is well optimized to reduce the amount of inelas-
 213 tic processes and to separate the spots in the ΔE —ToF plot, the energy
 214 resolution does not matter so much. When identifying the PID, i.e. by in-
 215 cluding the mass of the particles, the ΔE —ToF method cannot achieve at
 216 400 MeV/A an RIE better than 44% in average and can even attain 98.1%
 217 for tritons. ΔE — E and E —Range methods are well above it with 138.5%
 218 and 71.8% of mean values respectively. For the three methods, the values
 219 scale from lower to higher with the increasing beam energy, except for the

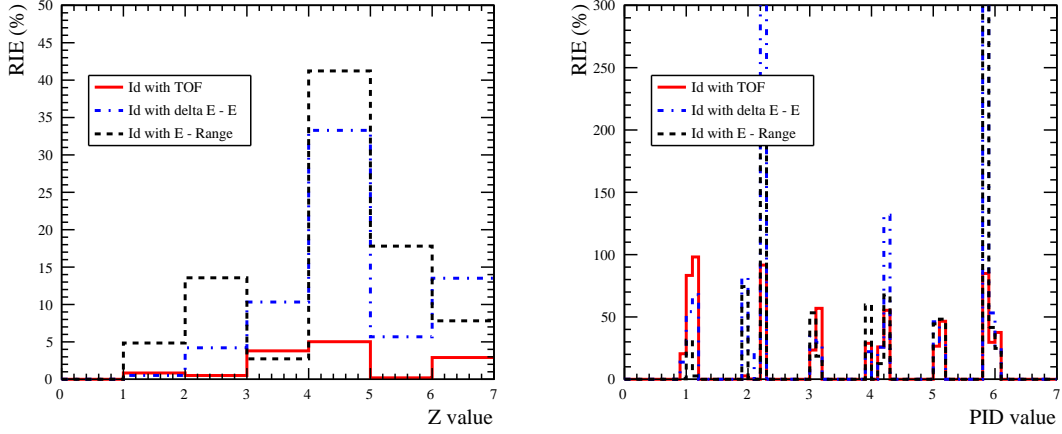


Figure 4: Relative identification errors versus Z and PID value for $E_{beam} = 400$ MeV/A. Red solid line, ΔE — E —ToF; blue dotted-dashed line, ΔE — E and black dashed line, ΔE —Range method.

220 E —Range method which acts differently at the lowest energy due to the
 221 sampling resolution at small ranges. Thus the other two techniques give
 222 acceptable results only up to $E_{beam} = 95$ MeV/A.

223 3.2. Energy evaluation

224 The relative energy distributions for the three methods are given in Fig. 5
 225 for a beam energy of 400 MeV/A. It is clear that even for well identified
 226 particles, an amount of energy is lost for a large number of ions, particularly
 227 for the ΔE — E and E —Range methods.

228 Table 4 summarizes the different R_{trunc} values for each technique and
 229 beam energy.

230 While R_{trunc} for the ΔE —ToF improves with the beam energy, from
 231 18.1% to 10.2%, the other two techniques tends to degrade it drastically.
 232 They are both in the same range of values to attain 38.2% and 32.8% of par-

Table 3: Averaged relative identification errors with respect to the method and beam energy. Maximum value in braces.

| Beam energy | Z identification error [max.] (%) | | | PID identification error [max.] (%) | | |
|----------------|-----------------------------------|---------------------|-----------------------|-------------------------------------|-------------------------|------------------------|
| (MeV/A) | ΔE — ToF | ΔE — E | ΔE — Range | ΔE — E —ToF | ΔE — E | ΔE — Range |
| 95 | 1.1±0.6 [2.1] | 1.6±1.5 [4.7] | 1.8±2.0 [6.0] | 5.5±4.6 [16.5] | 15.3±21.2 [86.0] | 93.9±221.2 [919.8] |
| 200 | 1.3±0.9 [2.4] | 5.2±4.8 [15.3] | 5.3±5.4 [16.4] | 16.0±13.9 [53.6] | 49.3±87.8 [339.0] | 31.9±47.0 [188.3] |
| 300 | 1.8±1.5 [4.2] | 7.1±6.3 [19.9] | 8.7±7.6 [24.1] | 41.4±28.8 [93.3] | 87.1±206.0 [861.3] | 37.0±42.0 [168.0] |
| 400 | 2.2±1.8 [5.0] | 11.3±10.7 [33.0] | 14.6±12.9 [41.2] | 44.0±30.0 [98.1] | 138.5±275.7 [1132.0] | 71.8±107.7 [1435.0] |

Table 4: Ratio of ions with truncated measured energy when well identified.

| Beam energy | R_{trunc} (%) | | |
|-------------|-----------------|------------------|-------------------|
| (MeV/A) | ΔE —ToF | ΔE — E | ΔE —Range |
| 95 | 18.1 | 11.2 | 10.2 |
| 200 | 6.0 | 14.1 | 13.4 |
| 300 | 2.6 | 24.9 | 23.4 |
| 400 | 1.6 | 38.2 | 32.8 |

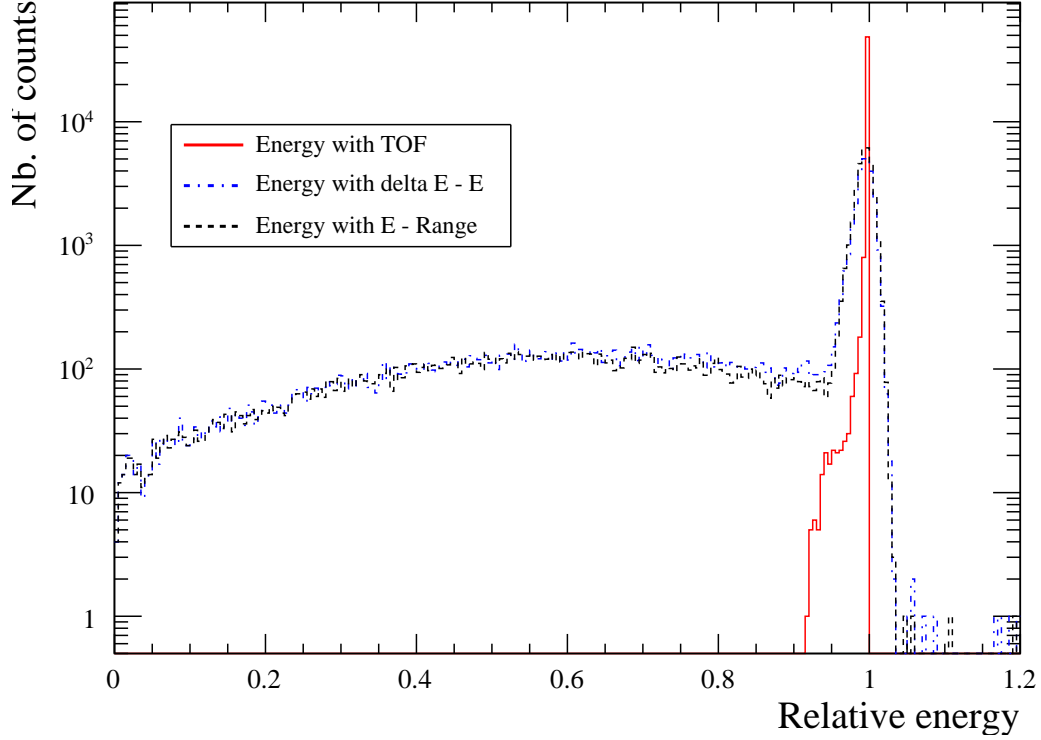


Figure 5: Relative energy distribution compared to the generated one for the three techniques with $E_{beam}=400$ MeV/A. Red solid line, ΔE —ToF; blue dotted-dashed line, ΔE — E and black dashed line, ΔE —Range method.

233 ticles with the energy truncated, for ΔE — E and ΔE —Range respectively.

234 4. Discussion

235 First, it is interesting to note that the E —Range method is in every
 236 energy cases the method that gives the highest RIE. This one is well suited for
 237 low velocity particles interacting in a gaseous detector, but offers very poor
 238 identification performances when used with a dense material and medium to
 239 high velocities particles.

240 To identify the mass of the ion in the given methods, one should measure
 241 the residual or total deposited energy. However, the measurement of the
 242 deposited energy is often degraded due to inelastic processes (i.e. the nucleus-
 243 nucleus collisions) which release a non negligible amount of energy through
 244 gamma or neutrons escape and, with a smaller contribution, Q value of the
 245 reaction. The lowered measured energy pollutes the identification process of
 246 lighter particles by in-between curves data points with strong horizontal lines
 247 for the ΔE — E plot or vertical ones for the E —ToF plot. Unfortunately, even
 248 if the cross-section of nuclear interactions is low compared to electromagnetic
 249 processes, the long traveling path of the particles in a rather large detector
 250 increases tremendously the probability of such reactions. This effect scales
 251 then with the particles kinetic energy worsening the RIE when increasing the
 252 beam energy.

253 As stated in section 2, the different method plots did not take into ac-
 254 count the beam particles interacting directly with the detection system. The
 255 amount of beam particles encountering no fragmentation processes in the
 256 target represents approx. 88% of the cases at 400 MeV/A with a 5 mm
 257 diameter target. They can then most likely have inelastic processes in the
 258 detector itself due to its dimensions, degrading the particle identification as
 259 mentioned previously. Figure 6 shows a comparison of the E —ToF plot with
 260 and without the beam particles at 400 MeV/A. It is clear that including
 261 beam particles in the identification process would result in artificially de-
 262 grading them and lead us to a different interpretation of the results, while
 263 the goal is to compare identification methods and not detection systems.

264 Even when well identified, a particle might have its measured energy

265 degraded. It can be attributed to two major effects: inelastic collisions mainly
 266 in the E stage and detector geometrical effects. Inelastic collisions may not
 267 be sufficient to misidentify the particle but the loss of energy by neutrons
 268 or gamma rays can be enough to truncate the measured energy. In the case
 269 of geometrical effects, the particles can escape by the sides due to lateral
 270 scattering, or by the back due to a high velocity (for light particles only).
 271 This last can be avoided by using a larger detector but would then increase
 272 the cost and the number of channels of the system.

273 The two techniques, ΔE — E and the ΔE —Range, have a very noxious
 274 incidence on the energy measurement. At $E_{beam} = 400$ MeV/A, the energy
 275 of more than 30% of the ions cannot be evaluated precisely, regardless of
 276 the energy resolution. In the end, this will result in larger error bars of the
 277 production cross sections relative to the energy.

278 In the case of the ΔE —ToF technique, one would think that R_{trunc} would
 279 increase with the beam energy. However, we can observe the opposite. This
 280 effect comes from the method to evaluate the number of ions with a truncated
 281 energy. The energy resolution evaluated by ToF scales with the beam energy
 282 (see eq. 8 in the case of non relativistic particles), a lower beam energy gives
 283 a better energy resolution. For the lowest beam energy, the evaluation of
 284 the FWHM of the peak centered at 1 gives a very small value. Then, more
 285 ions are included to be with a truncated energy outside of this peak. When
 286 increasing the beam energy, the FWHM peak value becomes larger and less
 287 ions are included in the R_{trunc} value.

$$\frac{\sigma_E}{E} = \frac{2\sigma_t}{ToF}, \quad \text{with} \quad \frac{1}{ToF} \propto E, \quad (8)$$

288 where σ_t is the coincidence time variance and taken as a constant.

289 It is then hard to tell to which lower limit to include ions in the R_{trunc}
290 value, that is why an arbitrary value of -5σ values was used regardless of the
291 method.

292 The same effect is however hidden in the other two techniques, resulting
293 in the opposite effect due to a worsening intrinsic energy resolution, follow-
294 ing an $E^{-1/2}$ trend, artificially improving results at low energy.

295

296 Finally, none of the presented methods is able to identify the particle
297 masses with a sufficiently good efficiency for a beam energy above 95 MeV/A
298 using only scintillating crystals. As for different types of detector, the goal
299 would always be to maintain an inelastic collisions rate as low as possible in
300 order to have the smallest error on the measurement of the deposited energy.

301 5. Conclusion

302 In this work, we have performed Monte Carlo simulations to test sev-
303 eral particle identification techniques. To be used in multi-fragmentation
304 experiments associated to carbon beams, we tested techniques based on the
305 measurement of the partial, the total or residual deposited energy, the range
306 as well as the time-of-flight of the particles. A detector composed of multiple
307 layers of scintillating inorganic crystal offers a good flexibility for testing the
308 identification techniques. The best of them, the ΔE — E —ToF method, can
309 only reach a PID RIE of 5.5% and 44% for a beam energy of 95 MeV/A and
310 400 MeV/A respectively. The other two methods give worse results. The use
311 of the ΔE —ToF method to obtain the charge of the particles associated to a

312 deflecting magnet is a more efficient method for mass measurements [19, 20],
313 not without an increase in the development costs.

314 References

- 315 [1] J. Dudouet, *et al.*, Comparison of two analysis methods for nuclear
316 reaction measurements of $^{12}\text{C} + ^{12}\text{C}$ interactions at 95 MeV/u for
317 hadron therapy, Nucl. Instr. and Meth. A 715 (0) (2013) 98 – 104.
318 doi:10.1016/j.nima.2013.03.038.
- 319 [2] R. Bass, J. Czarnecki, R. Zitzmann, Design study of a magnetically
320 focussed time-of-flight spectrometer for heavy ions, Nuclear Instruments
321 and Methods 130 (1) (1975) 125 – 133. doi:10.1016/0029-554X(75)90164-
322 0.
- 323 [3] E. Chulick, J. Natowitz, C. Schnatterly, A heavy ion identification
324 scheme based on semiempirical range-energy calculations, Nuclear In-
325 struments and Methods 109 (1) (1973) 171 – 175. doi:10.1016/0029-
326 554X(73)90462-X.
- 327 [4] D. Greiner, A versatile, high-resolution particle identifier-theory,
328 Nuclear Instruments and Methods 103 (2) (1972) 291 – 308.
329 doi:10.1016/0029-554X(72)90388-6.
- 330 [5] U. Amaldi, *et al.*, Construction, test and operation of a proton range
331 radiography system, Nucl. Instr. and Meth. A 629 (1) (2011) 337 – 344.
332 doi:10.1016/j.nima.2010.11.096.

- 333 [6] J. Asselineau, *et al.*, Performance of a Bragg curve detector for heavy
334 ion identification, Nuclear Instruments and Methods in Physics Research
335 204 (1) (1982) 109 – 115. doi:10.1016/0167-5087(82)90085-0.
- 336 [7] M. Mutterer, *et al.*, Breakthrough in pulse-shape based particle iden-
337 tification with silicon detectors, IEEE Transactions on Nuclear Science
338 47 (3) (2000) 756–759. doi:10.1109/23.856510.
- 339 [8] N. Le Neindre, *et al.*, Comparison of charged particle identification using
340 pulse shape discrimination and ΔE — E methods between front and rear
341 side injection in silicon detectors, Nucl. Instr. and Meth. A 701 (0) (2013)
342 145 – 152. doi:10.1016/j.nima.2012.11.005.
- 343 [9] S. Banerjee, *et al.*, Design and performance of a time-of-flight system
344 for particle identification at the fermilab collider, Nucl. Instr. and Meth.
345 A 269 (1) (1988) 121 – 133. doi:10.1016/0168-9002(88)90869-8.
- 346 [10] R. Strittmatter, B. Wehring, Fragment atomic-number identification us-
347 ing a gas ionization chamber in fission yield measurements, Nuclear In-
348 struments and Methods 166 (3) (1979) 473 – 481. doi:10.1016/0029-
349 554X(79)90537-8.
- 350 [11] S. Agostinelli, *et al.*, Geant4—a simulation toolkit, Nucl. Instr. and
351 Meth. A 506 (3) (2003) 250 – 303. doi:10.1016/S0168-9002(03)01368-8.
- 352 [12] M. D. Napoli, *et al.*, Carbon fragmentation measurements and valida-
353 tion of the geant4 nuclear reaction models for hadrontherapy, Physics
354 in Medicine and Biology 57 (22) (2012) 7651. doi:10.1088/0031-
355 9155/57/22/7651.

- 356 [13] J. T. M. de Haas, P. Dorenbos, Advances in yield calibration
357 of scintillators, IEEE Trans. Nucl. Sci. 55 (3) (2008) 1086–1092.
358 doi:10.1109/TNS.2008.922819.
- 359 [14] M. Pârlog, *et al.*, Response of CsI(Tl) scintillators over a large range in
360 energy and atomic number of ions. Part II: calibration and identification
361 in the INDRA array, Nucl. Instr. and Meth. A 482 (3) (2002) 693 – 706.
362 doi:10.1016/S0168-9002(01)01712-0.
- 363 [15] J. A. Mares, *et al.*, Scintillation response of Ce-doped or intrinsic scin-
364 tillating crystals in the range up to 1 MeV, Radiation Measurements
365 38 (4-6) (2004) 353 – 357, proceedings of the 5th European Confer-
366 ence on Luminescent Detectors and Transformers of Ionizing Radiation
367 (LUMDETR 2003). doi:10.1016/j.radmeas.2004.04.004.
- 368 [16] V. Andreev, *et al.*, A high-granularity scintillator calorimeter readout
369 with silicon photomultipliers, Nucl. Instr. and Meth. A 540 (2-3) (2005)
370 368 – 380. doi:10.1016/j.nima.2004.12.002.
- 371 [17] M. Moszyński, *et al.*, New photonis XP20D0 photomultiplier for fast
372 timing in nuclear medicine, Nucl. Instr. and Meth. A 567 (1) (2006) 31
373 – 35, proceedings of the 4th International Conference on New Develop-
374 ments in Photodetection. doi:10.1016/j.nima.2006.05.054.
- 375 [18] L. Tassan-Got, A New functional for charge and mass identifica-
376 tion in ΔE -E telescopes, Nucl. Instrum. Meth. B194 (2002) 503–512.
377 arXiv:nucl-ex/0103004, doi:10.1016/S0168-583X(02)00957-6.

- 378 [19] R. Pleskac, *et al.*, The FIRST experiment at GSI,
379 Nucl. Instr. and Meth. A 678 (0) (2012) 130 – 138.
380 doi:<http://dx.doi.org/10.1016/j.nima.2012.02.020>.
- 381 [20] K. YONEDA, SAMURAI A Large-Acceptance Spectrometer in RIBF,
382 Ch. 48, pp. 242–247. doi:[10.1142/9789814417952-0048](https://doi.org/10.1142/9789814417952-0048).

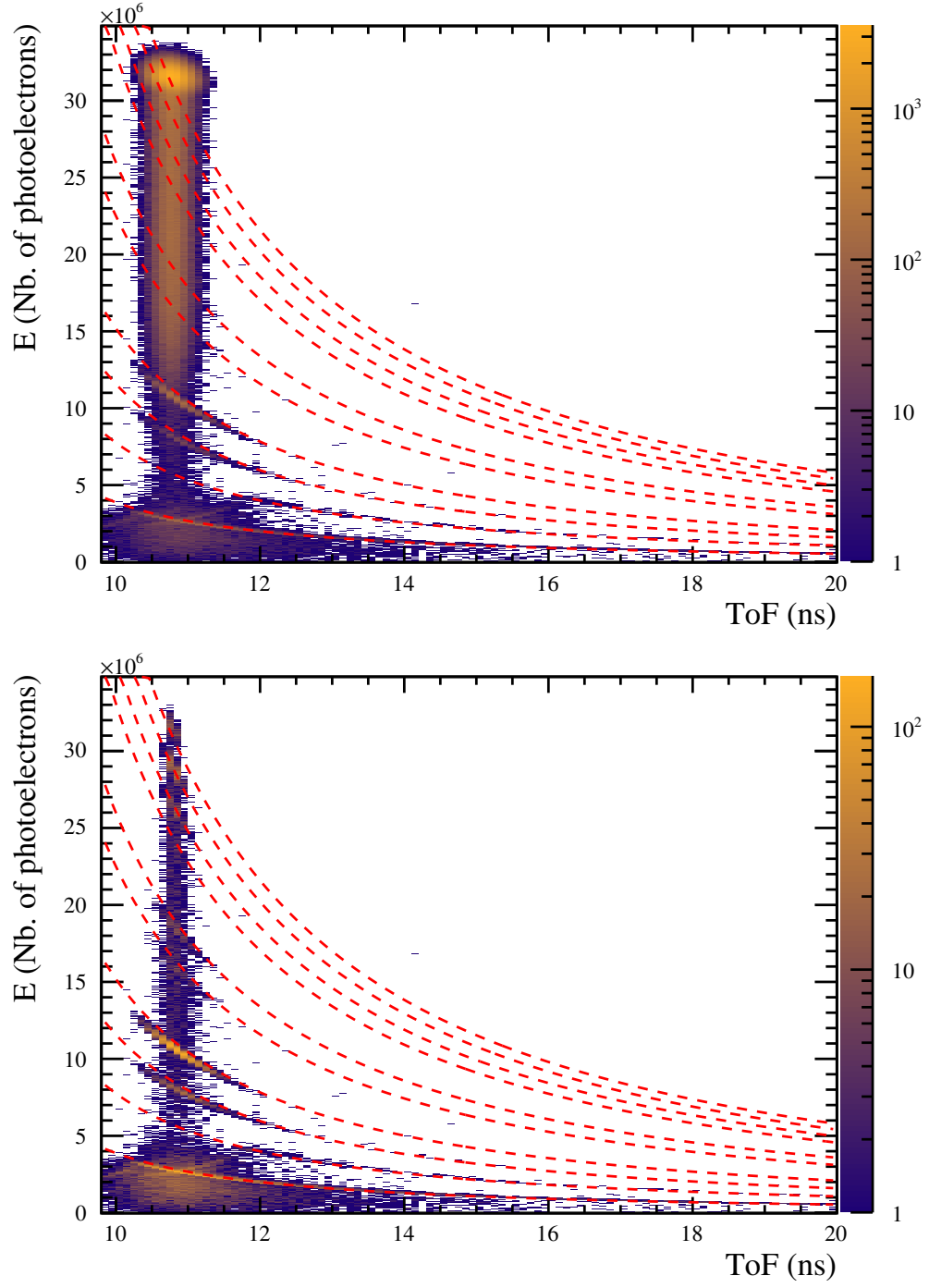


Figure 6: Comparison of the E —ToF plots with (top) and without (bottom) the beam particles at $E_{beam} = 400$ MeV/A.